Journal of Molecular Catalysis A: Chemical 420 (2016) 178–189

Contents lists available at ScienceDirect

Journal of Molecular Catalysis A: Chemical

journal homepage: www.elsevier.com/locate/molcata

(V)/Hydrotalcite, (V)/Al2O3, (V)/TiO2 and (V)/SBA-15 catalysts for the partial oxidation of ethanol to acetaldehyde

J.M. Hidalgo[a,*], Z. Tišler[a], D. Kubička[a], K. Raabova[b], R. Bulanek[b]

[a] Unipetrol Centre of Research and Education (UNICRE), Záluží 1, 436 70 Litvínov, Czech Republic
[b] Department of Physical Chemistry, Faculty of Chemical Technology, University of Pardubice, Studentska 573, 532 10 Pardubice, Czech Republic

ARTICLE INFO

Article history:
Received 14 January 2016
Received in revised form 20 April 2016
Accepted 21 April 2016
Available online 25 April 2016

Keywords:
Ethanol oxidation
Acetaldehyde
Vanadium
Titanium oxide
Hydrotalcite

ABSTRACT

Vanadium-based catalysts have been investigated in the partial oxidation of ethanol to acetaldehyde with the aim of understanding relationship between vanadium structure and acetaldehyde productivity. Hydrotalcite, Al_2O_3, TiO_2 and SBA-15 with and without a 5% of vanadium content were prepared to study the oxidative dehydrogenation of ethanol. They were characterized by XRF, TPR (H_2), NH_3-TPD, CO_2-TPD, RAMAN, UV-vis, Nitrogen physisorption, XRD and SEM. The most easily reducible catalysts (as determined by TPR) were the most active ones. In the low temperature region (150 °C), the most active catalyst was the V/TiO_2 which presented stable activity in the production of acetaldehyde up to TOS = 200 h. On the contrary, in the high temperature region (250 °C), the most active catalyst was the V/Al_2O_3catalyst. The most promising result was obtained over V/TiO_2 catalyst that afforded a total ethanol conversion of 60.4%wt. and a selectivity to acetaldehyde of 76.2%wt. at TOS = 164 h and T = 150 °C. Also, hydrotalcite was tested for the first time for this type of reaction providing a conversion lower than 7%wt. with a selectivity of 100%wt. to acetaldehyde at T = 150–225 °C.

1. Introduction

Green production of chemicals is in the spotlight both academic and industrial research worldwide with the aim to decrease the fossil carbon footprint. As a result, platform chemicals from biomass have attracted significant attention in the recent years. Ethanol (bio-ethanol) produced by fermentation of sugars is one of the most important platform chemicals. As a result of the legislation-driven increase in demand for biofuels, the production of bioethanol has significantly increased (from ca. 10 billion US gallons in 2005 to ca. 15 billion US gallons in 2007 with predicted increase to 30 billion US gallons in 2016 [1]) over the past years resulting in a drop in its price and increased availability. Currently, application of bio-ethanol as a fuel accounts for around 75% of the total amount of bio-ethanol produced [2] but the decrease in price makes the more extensive use of bio-ethanol for the production of the higher-value bulk chemicals very attractive. The use of bio-ethanol could lead also to higher CO_2 savings than its use as a fuel [3].

Acetaldehyde is an important intermediate used for the production of various bulk chemicals, including acetic acid, acetic anhydride, ethyl acetate, per acetic acid, butanol, 2-ethylhexanol, pentaerythritol, chlorinated acetaldehydes, glyoxal, alkyl amines, pyridens and others [4]. In 2012 the global acetaldehyde consumption was divided mainly between the production of pyridine and pyridine bases (16% of total production), pentaerythritol (16% of total production), acetate esters (14% of total production), the remainder being used for the synthesis of 1,3-butylene glycol, croton aldehyde and glyoxal, along with some smaller-volume derivatives [4,5]. Recently, new applications for acetaldehyde have been proposed. As acetaldehyde can be synthesized from various stating materials the choice of it depends on its price and its availability. Today, mainly ethylene is used due to its wide availability and low price for synthesis of acetaldehyde by direct oxidation, while ethanol and acetylene are used only to a small extent. Ethylene oxidation to acetaldehyde, so called Wacker process, developed in late 1950s, consists of oxidation of ethylene using aqueous $PdCl_2$ and $CuCl_2$ as catalysts. Although this reaction is characterized by advantages such as small amount of $PdCl_2$ required for the reaction and regeneration of the catalyst, there are some drawbacks which make this reaction economically quite demanding. Among them belongs i) the need of using corrosive resistant materials together with expensive titanium reactor tubing or ii) need of purification of waste air and treatment of wastewater, in order to remove acetaldehyde, unconverted ethylene and mainly chlorinated hydrocarbons, which are highly toxic and show antimicrobial activity. Therefore, they must be treated before

* Corresponding author.
E-mail address: jose.hidalgo@unicre.cz (J.M. Hidalgo).

http://dx.doi.org/10.1016/j.molcata.2016.04.024
1381-1169/

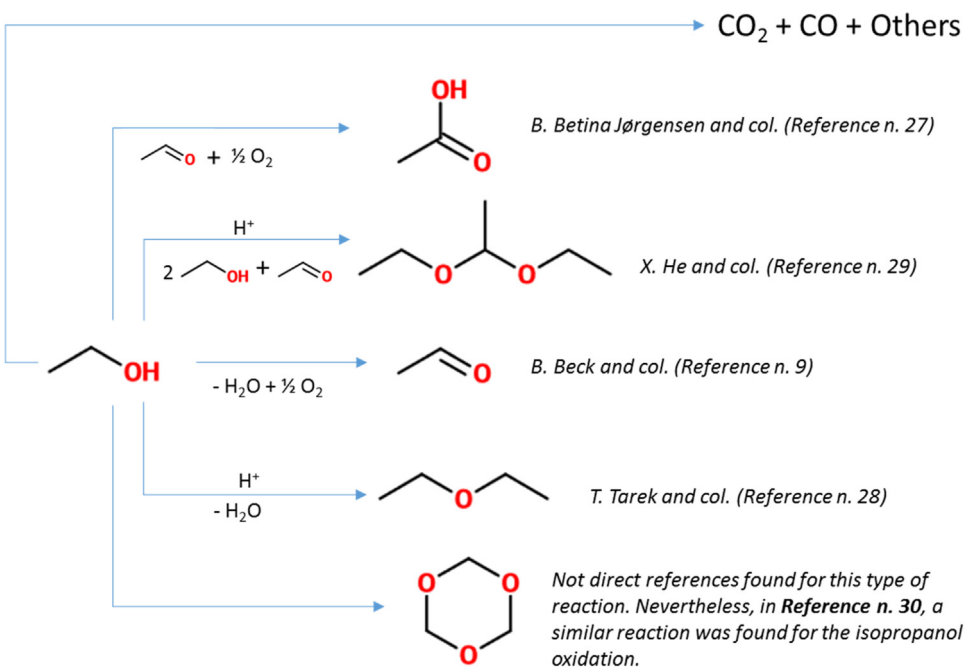

Scheme 1. Different products obtained from the partial oxidation of ethanol.

entering the wastewater plant to render them biologically degradable [4,6,7]. Thus, the acetaldehyde production via the oxidative dehydrogenation (ODH) of ethanol could be a promising alternative to the Wacker process, occurring more simply in a single step and in tubular reactors, if high activities and selectivities can be achieved under mild conditions.

Supported vanadium oxide catalysts have been studied by different authors with the objective of elucidating their performance in the oxidation of ethanol [7–9]. The oxidation of ethanol to acetaldehyde is currently investigated with the aim of replacing the conventional processes based on hazardous agents such as chromate or permanganate [10]. Vanadium-based catalysts have been also used and studied for the partial oxidation or oxidative dehydrogenation reactions [3,5]. Besides, the dispersion and nature of the vanadium over the adequate support is an important issue to obtain a high catalytic activity [11]. Several catalysts with some vanadium content were characterized with the aim of studying the type of vanadium present on their surface and its role in the partial oxidation of ethanol using high space velocity. Here we compare the performance of some vanadium oxides supported on alumina, titania, hydrotalcite and SBA-15 (SiO_2) supports.

Different authors used vanadium catalysts for the oxidation of ethanol. Chimentao et al. [12] studied the oxidation of ethanol to acetaldehyde over Na-promoted vanadium oxide catalysts obtaining an ethanol conversion of 20% with a selectivity to acetaldehyde of 95% at 250 °C (the ethanol was vaporized before feeding it to the reactor). Hsiu-Mei Lina et al. [13] used V_2O_5/TiO_2/MCM-41 catalysts for the catalytic oxidation of ethanol at 300 °C obtaining a conversion of 60% and a selectivity to acetaldehyde of 70%. In this case, a mixture of ethanol and air was used with WHSV = 2.5 h^{-1}. Kannan et al. [14] oxidized ethanol over microporous vanadium silicate molecular sieves with MEL structure at 300 °C and WHSV = 2.6 h^{-1} obtaining a total conversion of 55% with a selectivity to acetaldehyde of 67%. The published work from Tóth et al. [15] was an example of using different metal oxides for the oxidation of ethanol. Nevertheless, in this work the metal used was the Rh and not the V. The total conversion in this case for the most active catalyst was 97% and the selectivity to acetaldehyde 13.8%. SBA-15 materials are being used mainly for other purposes different than the partial oxidation of ethanol. Nevertheless, some works were published such as the research from Gayoung Lee et al. [16] who used V_2O_5/SBA-15 materials for the oxidation of ethanol with the aim of producing hydrogen gas. Guoan Du et al. [17] used vanadium grafted SBA-15 for the oxidation of methanol but not for ethanol and Li et al. [18] used Ni/SBA-15 for the steam reforming of ethanol.

Many works informed about the characterization of the vanadium supported over different metal oxides [18–26]. These studies were a source of information which was used for the characterization of the catalysts tested in this work. An aim of this work was the characterization and obtaining a highly active and stable catalyst for the partial ethanol oxidation to acetaldehyde. In the Scheme 1 are represented the possible products which could be obtained from the oxidation of ethanol [9,27–29]. The acetaldehyde is the suitable product in this case. Nevertheless, the acetaldehyde diethyl acetal could be produced by the reaction between the ethanol and the acetaldehyde as described by He et al. [29]. Other possible products could be the acetic acid as consequence of the oxidation of the acetaldehyde [27] or the diethyl ether by the dehydration reaction of ethanol.

2. Experimental

2.1. Materials

Eight catalyst samples were prepared to study the oxidative dehydrogenation (ODH) of ethanol: hydrotalcite (HTC), Al_2O_3, TiO_2 and SBA-15 and their respective vanadium containing catalysts, i.e. V/HTC, V/Al_2O_3, V/TiO_2 and V/SBA-15.

Two commercial supports – TiO_2 (Euro Support Manufacturing Czechia s.r.o.) and γ-Al_2O_3 spheres (Sasol, 1 mm diameter) – and two in-house prepared supports – HTC and SBA-15–were prepared and used. The commercial supports were used after proper activation by drying and calcination. Mg/Al hydrotalcite with Mg/Al ratio equal to 3:1 was synthesized according to the procedure described by Kikhtyanin et al. [31] using of magnesium nitrate (99% wt., Lach-Ner s.r.o.), aluminium nitrate nonahydrate (98%wt., Lach-Ner s.r.o.), potassium hydroxide (99%wt., Lach-Ner s.r.o.) and potassium carbonate (99%wt., Lach-Ner s.r.o.). Mesoporous silica SBA-15

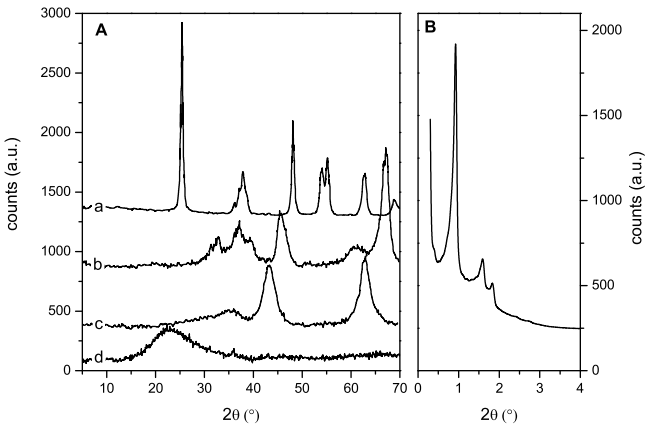

Fig. 1. (A) Wide angle XRD patterns of the vandium catalysts: a – V/TiO_2, b – V/Al_2O_3, c – V/HTC and d – V/SBA-15. (B) Small angle diffraction pattern of V/SBA-15.

support was synthesized according to the method reported by Zukal et al. [32] by using of tetraethyl orthosilicate (reagent grade 98%, Sigma-Aldrich), Pluronic® P-123 (purchased from Sigma Aldrich), hydrogen peroxide (30% wt. in water solution, Lach-Ner s.r.o.) and hydrochloric acid (35% wt., Lach-Ner s.r.o.).

The vanadium was added by incipient wetness impregnation method using ammonium vanadate (99%wt., Lach-ner s.r.o.). The precursor was added to the support in such amount to obtain 5%wt. of vanadium in the final catalyst. It was dissolved in a diluted solution of hydrogen peroxide (ratio hydrogen peroxide (30%wt. aqueous solution, Lach-ner s.r.o.) and demineralized water 1:4) and then added to 20 g of dried supports (TiO_2, Al_2O_3, HTC and SBA-15, respectively). The impregnated samples were dried at 120 °C overnight and then calcined at 450 °C for 6 h (heating ramp: 2 °C/min from room temperature to 450 °C).

2.2. Characterisation of catalysts

The composition of the catalysts was ascertained by X-ray fluorescence analysis (XRF) of the catalyst powder using a Philips PW 1404 with Rh cathode. The results were evaluated using the UniQuant software.

The crystallographic structure of the catalysts was determined by examining the X-ray diffraction (XRD) patterns of the powder samples obtained by using a Philips MPD 1880 applying CuKα radiation (λ = 1.5406 Å). The step size of 0.04° and a step time of 1 s were used. The patterns were collected over the 2θ range from 5° to 70° and evaluated by using the XíPert HightScore Plus Software version 2. 1b.

The specific surface area (BET) of the catalysts was determined by N_2 adsorption/desorption at −196 °C by using an Autosorb iQ. All samples were dried before the analysis in a glass-cell at 200 °C under vacuum for 16 h.

SEM images were obtained by using a scanning electron microscope (SEM) JSM-7500F with a cold cathode – field emission SEM (parameters of measurements: 1 kV, GB high mode).

The UV–vis diffuse reflectance spectra of diluted and subsequently dehydrated samples were measured using a Cintra 303 spectrometer (GBC Scientific Equipment, Australia) equipped with a Spectralon-coated integrating sphere using a Spectralon coated discs as a standard. The spectra were recorded in the range of the wavelength 190–850 nm with resolution of 1 nm scanned by the rate of 100 nm/min. The samples were diluted by the pure silica (Fumed silica, Aldrich) in the ratio 1:100 in order to obtain better resolution of individual spectral bands and the linear dependence of spectral area on the concentration of vanadium (for more details see ref. [33]) All samples were granulated and sieved to fraction of size 0.25–0.5 mm, dehydrated before the spectra measurement and oxidized in the glass apparatus under static oxygen atmosphere (16–18 kPa) in two steps: 120 °C for 30 min and 450 °C for 60 min. Subsequently, the sample was cooled down to 250 °C and evacuated for 30 min. After the evacuation, the samples were transferred under vacuum into the quartz optical cuvette 5 mm thick and sealed under vacuum. This procedure guaranteed complete dehydration (independently checked by measurement of overtones of OH group vibration on UV–vis-NIR spectrometer) and defined oxidation state of vanadium for all catalysts (presence of vanadium (IV) was tested independently by ESR without any measurable signal under the same condition like DR UV–vis pretreatment).

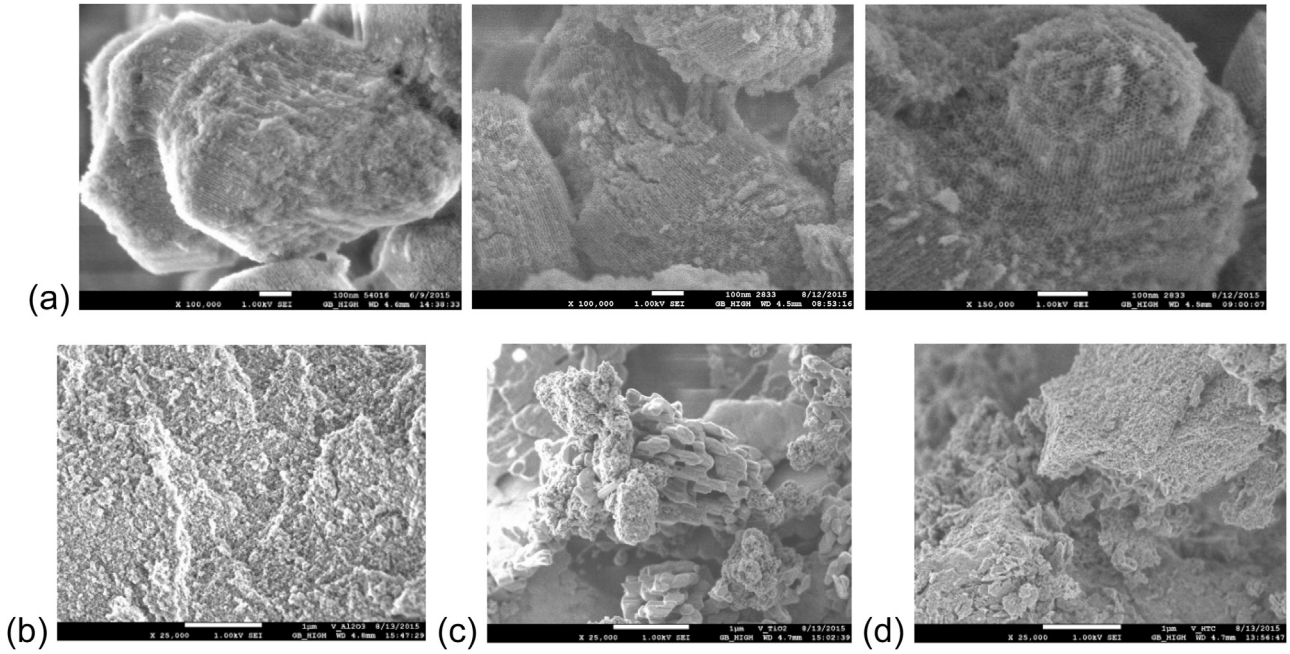

Fig. 2. SEM images. (a) V/SBA-15(x100,000 and x150,000); (b) V/Al_2O_3(x25,000); (c) V/TiO_2 (x25,000);(d) V/HTC (x25,000).

All Raman spectra were measured under dehydrated conditions. The dehydration and oxidation protocol was the same as for DR UV–vis spectra measurement (see above). The Raman spectra were measured in glass cuvette by Nicolet DXR Smart Raman spectrometer equipped with CCD detection. Spectra were excited by Smart Excitation Laser (Thermo Scientific) with laser wavelength at 780 nm. The spectra were recorded by collecting of 2000 scans (scan time was 2 s with resolution 2 cm-1 in all cases). The laser power delivered to the sample varied depending on the sample concentration (max 50 mW). Spectrograph aperture was 50 μm slit (equivalent to laser spot size approximately 3.1 μm at the sample).

The reducibility of the vanadium species in the vanadium-containing catalysts was determined by H_2-TPR using an AutoChem 2920 (Micromeritics) instrument. 100 mg of sample (50 mg for V/SBA-15) in a quartz U-tube were oxidized in oxygen flow at 450 °C (2 h) prior to the measurement. Reduction was carried out at T = 25–900 °C with a temperature ramp of 10 °C/minute under reducing gas flow (5 vol.% H_2 in Ar). The changes of hydrogen concentration were monitored by a TCD detector.

Acid-base properties of materials were characterized by means of CO_2 and NH_3 temperature programmed desorption (TPD) using Autochem 2920 (Micromeritics, USA). Typically 100 mg of sample in a quartz U-tube reactor was pretreated in He to 500 °C with temperature ramp of 10 °C/min. In the case of NH_3-TPD, the sample was cooled to 180 °C and then it was saturated with ammonia by flow of 25 ml/min of 10 vol.% NH_3/He for 30 min. Subsequently, the gas was changed to helium (25 ml/min) in order to removed physically/weakly adsorbed ammonia and flushing out until the baseline was constant (60 min). After this procedure the temperature was increased to 500 °C with a rate of 15 °C/min to obtain the NH_3-TPD curves. In the case of CO_2-TPD, the sample pretreatment was the same as in the case of NH_3-TPD. After the pretreatment the sample was cooled to 50 °C and the gas was switched to gas mixture of 10 vol.% CO_2/He (25 ml/min). The sample was saturated by CO_2 for 30 min. After that the gas was changed to helium and left for another one hour at 50 °C in flow of helium in order to remove weakly adsorbed molecules. TPD curves were obtained by increasing the temperature from 50 °C to 500 °C with the ramp of 15 °C/min.

2.3. Catalytic tests

All the catalysts were tested with the aim to determine their activity and selectivity in the oxidation (oxidative dehydrogenation, ODH) of ethanol. A trickle bed reactor (stainless steel 316) with a length of 1000 mm was used. The reaction was carried out using 2.2 g of catalyst. The catalyst was prepared in a form of pellets with a diameter of 0.5 mm. The catalyst bed had a length of 301 mm and was located in the central part of the reactor. The catalyst and silicon carbide (0.5 mm particles) were mixed thoroughly (20 ml SiC + 2.2 g of catalyst) and loaded into the reactor. Finally, the remaining free volume of the reactor was filled with silicon carbide. Air flow, used for the catalytic reaction, was fed directly (activation 1 h at 400 °C; 5 °C/min from room temp.) or mixed with feedstock before entering the reactor. All catalysts were tested at 150, 200, 225 and 250 °C using 5 NL/h air flow, 1 bar of pressure and 5 g/h of ethanol. V/TiO_2 catalyst was also tested using larger times of reaction. The products were collected in two collectors, the first one cooled by water to room temperature and the second one cooled to 0 °C. Each two collected liquid samples were mixed to one sample and analysed using a GC-FID "Agilent 7890A" and GC-OFID "Agilent-Wasson-ECE Instrumentation". Gaseous products were analysed by the method "Refinery Gas Analysis" RGA (Agilent Technologies) with a GC 7890A Agilent (USA). The products were identified by using standard reference compounds along with GC–MS analyses using Thermo Scientific ITQ 1100 unit.

3. Results and discussion

3.1. Characterization

3.1.1. XRF, XRD and nitrogen physisorption

The elemental composition of the supports and supported vanadium catalysts obtained by XRF is presented in Table 1 and Table 2, respectively together with their BET areas determined by physisorption of N_2. All supports were pure with minimum content of admixtures – SiO_2 in Al_2O_3 and Al_2O_3 in TiO_2. The Mg/Al atomic ratio of the prepared HTC was 2.1:1. The BET area was similar for all supports (approx. 160 m^2/g) with exception of SBA-15 that exhibited a large surface area due to its ordered mesoporous structure (Table 1).

All of the vanadium-doped catalyst samples except V/HTC contained approximately the desired amount of vanadium pentoxide (8 ± 0.5%wt.). The vanadium content in the V/HTC sample was significantly larger than the desired one because hydrotalcite was dehydrated during calcination of impregnated sample resulting in a significant weight loss of support (approximately 50%wt.). The specific surface area (SSA) of V/Al_2O_3 was the same as of the support, whereas the other catalysts exhibited drop in the SSA in the range from 30 (for V/HTC) to 66 rel.% (for V/TiO_2) relative to their parent supports. Some changes in the SSA are very frequent for supported catalyst, especially in the case of porous materials, due to the partial blocking of the pores, occupation of part of the space in the pores by host species or partial changes in morphology of the particles during impregnation and subsequent calcination.

The XRD patterns of the catalysts are shown in Fig. 1. All of the samples show peaks attributable to the oxidic supports and no crystalline phases of vanadium oxides were observed. V/TiO_2 (see pattern a in Fig. 1A) exhibitstypical set of diffractions for anatase phase (at two theta 25.3, 37.05, 37.9, 38.7, 48.16, 54.05, 55.2, 62.9 and 68.98°) and no diffraction lines for rutile can be seen (Fig. 1A pattern a). V/Al_2O_3 catalyst exhibits relatively broad diffraction lines at 19.6, 32.2, 36.7, 39.5, 45.5, 61.4 and 67.25° attributable to gamma alumina (Fig. 1A pattern b). XRD pattern of V/HTC consists of two broad peaks at 43.1 and 62.9° typical for MgO (Fig. 1A pattern c). Low-intensity broad feature between 30 and 40° have been previously attributed to partially crystalized Mg orthovanadate. [34,35] V/SBA-15 catalyst exhibits only a very broad band between 15 and 30° which belongs to amorphous silica (see Fig. 1A pattern d). Small angle XRD pattern of V/SBA-5 (Fig. 1B) exhibited three peaks at 0.919, 1.593 and 1.836 that can be indexed on a 2-D hexagonal lattice.

3.1.2. SEM

SEM images of V/SBA-15 show lenticular particles of approx. 0.5 μm in diameter with an ordered porous structure typical of a SBA-15 material (Fig. 2(a)). For V/Al_2O_3 and V/HTC, the presence of very small particles clustered to agglomerates is visible in the images (Fig. 2(b) and (c)). For the TiO_2 structure, two types of apparent structures were identified; the elongated structure could be assigned to ordered TiO_2 and the "sponge-like" form to the amorphous titanium oxide formed in suspense during the impregnation of vanadium on the surface. No separate particles of vanadium oxide were observed in any of the catalysts.

3.1.3. UV–vis and raman studies

UV-vis spectra of the dehydrated catalysts are presented in Fig. 3. All catalysts exhibit several absorption bands in the region 2–6 eV which are conventionally attributed to the ligand to metal charge-transfer transition of the $O \rightarrow V^V$ type. It must be noted that

Table 1
XRF elemental analysis and specific surface area for supports.

Support	XRF (%wt.)					Specific surface area (m^2/g)
	Al_2O_3	MgO	SiO_2	TiO_2	Sum	
Al_2O_3	99.1	–	0.3	–	99.4	153
TiO_2	1.2	–	–	97.2	98.4[a]	173
SBA-15	–	–	99.8	–	99.8	645
HTC	37.3	62.2	–	–	99.5	176[b]

[a] 1%wt. of SO_3 should be added to the total amount. Hence, the real sum is 99.4%wt.
[b] The surface area corresponds to the support pre-treated under the same conditions as vanadium catalysts.

Table 2
XRF elemental analysis, specific surface area and energy of absorption edge for catalysts with vanadium.

Catalyst	XRF (%wt.)						Vanadium content (%wt.)	ε_0 (eV)	Specific surface area (m^2/g)
	V_2O_5	MgO	Al_2O_3	TiO_2	SiO_2	Sum			
V/Al_2O_3	7.5	–	92.2	–	–	99.7	4.2	2.50	154
V/TiO_2	8.8	–	1.2	87.9	–	97.9	4.9	2.71	76
V/SBA-15	7.4	–	–	–	89.2	96.6	4.2	3.26	399
V/HTC	19.9	54.9	24.7	–	–	99.5	11.1	3.10	122

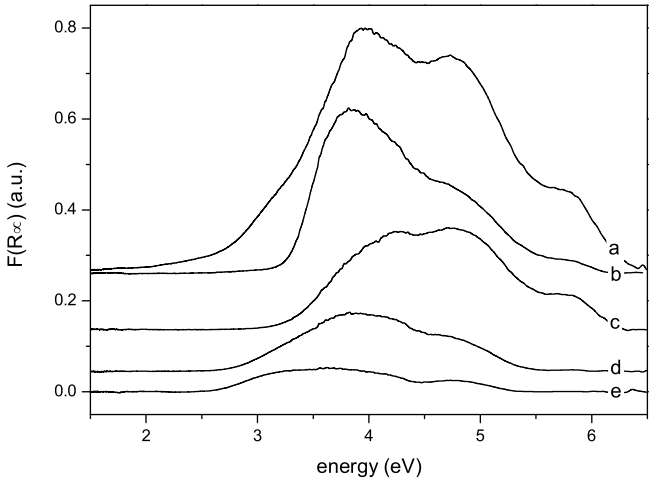

Fig. 3. Diffuse reflectance UV–vis spectra of dehydrated vanadium catalysts. a – V/TiO_2, b – TiO_2, c – V/SBA-15, d – V/HTC, e – V/Al_2O_3.

parent TiO_2 support exhibits strong absorption in the UV region overlapping intensively with the absorption bands of vanadium species (see Fig. 3 spectrum b). The other supports exhibit only negligible intensity of absorption bands and therefore they are not presented in Fig. 3 for the sake of its brevity and clarity. The methodology and assignment of signals used for UV–vis spectra was the same as that described previously by M. Setnička et al. [33,36,37]. The degree of dispersion of vanadium species was assessed by the evaluation of the energy of the edge (ε_0) using Tauc's law (see Table 2). It is evident that the catalysts differ in distribution of vanadium species reflected in the differences in the value of the energy of the edge. The highest ε_0 exhibits V/SBA-15 catalyst. The relative amount of the monomeric and oligomeric tetrahedrally coordinated species for V/SBA-15 catalyst was a 16% and 84%, respectively. The other catalysts exhibit significantly lower values of ε_0 laying below the value of the metavanadate ε_0 (model compound for linearly polymerized tetrahedrally coordinated units with V—O—V bonds, ε_0 = 3.13 eV) indicating thus the presence of 2D octahedral oxidic species. This is in agreement with the presence of 995 cm^{-1} Raman band in the spectra of V/Al_2O_3 and V/TiO_2 (see Fig. 4 for details). V/HTC catalyst exhibits ε_0 equal to 3.1 eV that is in good accordance with the spectra reported in literature. [38] Value of ε_0 is given by the superposition of the present isolated surface vanadium species and Mg-vanadates (especially $Mg_3V_2O_8$ as evidenced by Raman spectroscopy see Fig. 4)

From the Raman spectra (Fig. 4), we could conclude that the samples contained wide variety of surface species ranging from

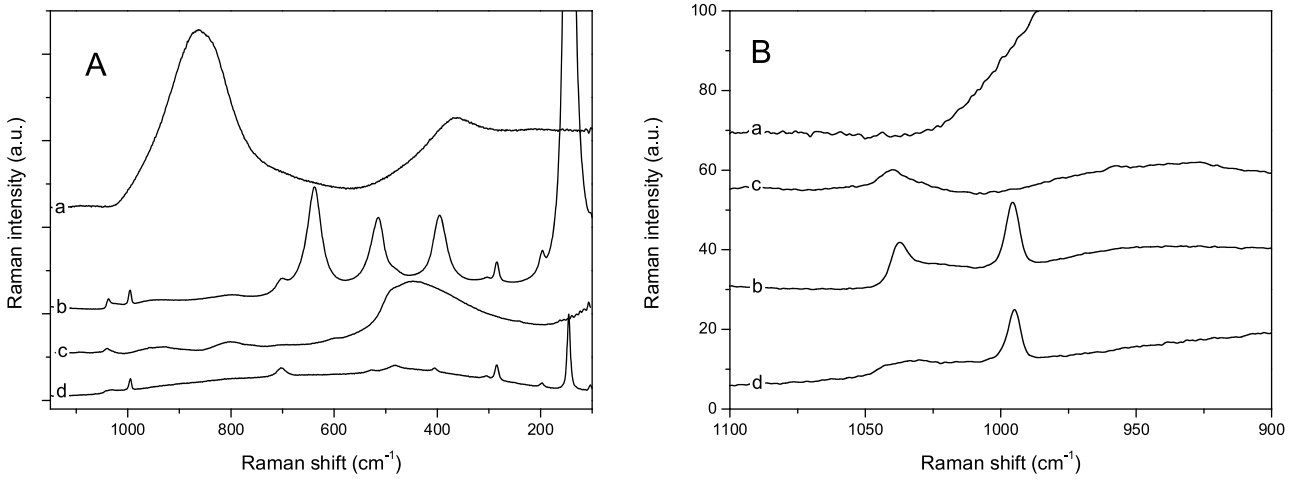

Fig. 4. Raman spectra of the dehydrated vanadium catalysts in the range of 100–1200 cm^{-1} (A) and the detail of the spectra in the range of VO vibration around 1000 cm^{-1} (B). a – V/HTC, b – V/TiO_2, c – V/SBA-15, d – V/Al_2O_3.

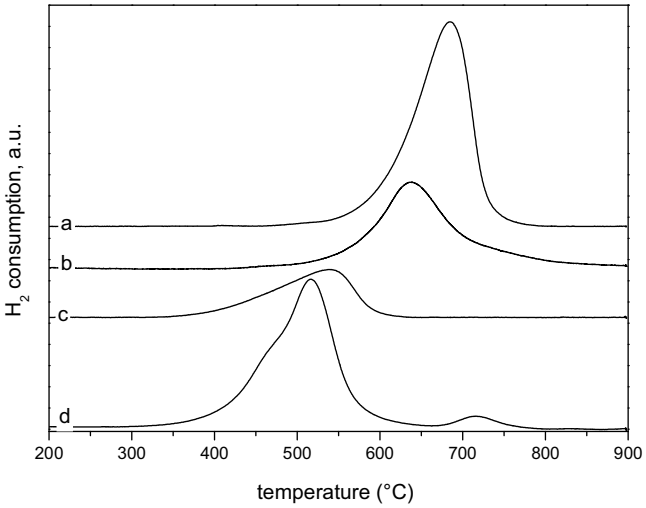

Fig. 5. H_2-TPR patterns for vanadium catalysts, a – V/HTC, b – V/SBA-15, c – V/Al_2O_3, d – V/TiO_2.

isolated monomeric VO_4 species and oligomeric species with Td coordination to V_2O_5 microcrystallites with octahedral coordination. The distribution of species differed significantly from support to support. V/SBA-15 catalyst exhibited Raman signals at 1040 cm^{-1} with a shoulder at low-Raman shift side evidencing the presence of well-dispersed VO_x species with tetrahedral coordination. No Raman signal at 995 cm^{-1} was detected indicating thus the absence of V_2O_5 microcrystallites. Surprisingly, this band (995 cm^{-1}) is clearly visible together with other signals at 702, 524, 407, 301, 282, 197 and 145 cm^{-1} in the spectra of V/TiO_2 and V/Al_2O_3 which indicates the presence of octahedral oxidic species in these catalysts. However, no bands at 2.6 and 3.1 eV are visible in the DR UV–vis spectra of these samples (cf. spectra in Fig. 3). It is well-know that Raman spectroscopy is much more sensitive as compared with UV–vis spectroscopy, therefore the presence of Raman signals at 995 cm^{-1} and the absence of UV–vis bands at 2.6 and 3.1 eV is not in contradiction. It means that the content of oxidic species is relatively low, under the detection limit of UV–vis spectroscopy, but above the detection limit of Raman spectroscopy [24]. Both V/TiO_2 and V/Al_2O_3 exhibit Raman signals at around 1040 cm^{-1} with a shoulder at 1028 cm^{-1} proving the presence of tetrahedrally coordinated vanadium species. Comparison of these Raman signal shapes indicate a broader distribution of vanadium species in the case of the alumina catalyst. It must be noted that the strong Raman signals at 638, 515, 396 and 143 cm^{-1} in the spectrum of V/TiO_2 belong to the spectrum of the support (anatase). [39] V/HTC exhibits quite different character of Raman spectra. Two broad Raman signals at 864 and 366 cm^{-1} dominate the spectrum. According to the literature, these bands can be ascribed to the symmetric stretching mode (864 cm^{-1}) and deformation mode (366 cm^{-1}) of $Mg_3V_2O_8$ orthovanadate formed in the catalysts by solid-state reaction of the vanadium precursor with MgO oxide during the calcination of the catalyst. The broadening of the band at 864 cm^{-1} results from the overlap of several bands, especially band at 825 cm^{-1} belonging to V-O-Mg vibration of the tetrahedrally coordinated VO_4 species, 860 cm^{-1} band assigned to $Mg_3V_2O_8$ and the band above 900 cm^{-1} attributed to $Mg_2V_2O_7$ [38–41].

3.1.4. Temperature programmed reduction (TPR)

TPR patterns are shown in Fig. 5. V/TiO_2 showed two reduction peaks (at 516 and 717 °C) with a shoulder at 462 °C which reflects the presence of VO_X units with a different degree of polymerization and/or different coordination environment. High-temperature reduction peak can be attributed to the reduction of small amount of the oxide-like species responsible for the Raman peak at 995 cm^{-1}. The other catalysts exhibit only one asymmetric reduction peak. The position of its maximum decreased in the following order: V/HTC (683 °C) > V/SBA-15 (638 °C) > V/Al_2O_3 (539 °C). The character and reduction temperatures for V/Al_2O_3 and V/SBA-15 are typical and attributable to the reduction of tetrahedrally coordinated VOx surface species. The very high reduction temperature for V/HTC catalyst (685 °C) evidences the presence of hardly reducible magnesium vanadate domains. By comparison of the TPR patterns, it can be noted that vanadium on TiO_2 is the most easily reducible one whereas vanadium on the calcined hydrotalcite support exhibits the lowest reducibility among all catalysts. The changes in the oxidation state of the vanadium, calculated from the consumption of hydrogen, are summarized in Table 3. The oxidation state change was found to be between 1.3 and 2.1. The values very close to 2 (for silica and titania catalysts) evidence the almost quantitative reduction of vanadium from state V^V to V^{III}. The significantly lower hydrogen consumption in the case of V/HTC catalyst (1.3) can be caused either by the formation of the hardly reducible Mg vanadates or by the inaccuracy in the determination of the vanadium amount in the sample insert into reactor caused by the uncontrolled state of hydration/dehydration of catalyst during weighing.

3.1.5. Temperature programmed desorptions (TPD)

NH_3-TPD characterization was conducted to survey the acidity of each catalyst and appropriate support (Fig. 6) All materials are showed a broad NH_3 desorption peak stretched in a wide range from 200 to 450 °C corresponding to the intermediate and stronger acid sites (it must be noted that ammonia from the weakest sites was removed before TPD experiment by flushing the sample by the carrier gas at 180 °C for 60 min). All TPD profiles exhibit the maximum of desorption peaks in a relatively narrow range of temperatures between 260 and 290 °C, but differ in the shape and width of the peaks which indicates variation in the distribution of the strength of acid sites. It can also be observed (Fig. 6) that the characteristics and the amount of acid sites varied when vanadium was deposited by impregnation on the surface of supports. The maximum of the TPD peak is slightly shifted to the lower temperature evidencing weakening of acid sites after impregnation with vanadium. In addition, a distinct TPD peak at 386 °C has developed in the case of V/TiO_2. Quantitative analysis (Table 3) clearly shows that SiO_2 support contains the lowest amount of acid sites. On the other hand, TiO_2 exhibits the largest amount of desorbed ammonia and the desorption takes place up to the highest temperature evidencing a high content and high population of strong acid sites. This high strength of acid sites on the surface of TiO_2 could be associated with the presence of traces of sulfur in the material acting as strong acid site.

CO_2-TPD profiles are shown in Fig. 7. Three different regions of CO_2 desorption can be distinguished: the desorption peak at about 100 °C can be attributed to the desorption of weakly bonded CO_2, peaks between 150 and 300 °C belong to CO_2 desorption from sites of medium strength, and finally the desorption at high temperatures (above 350 °C) originates from strong sites. Acidic supports (SBA-15 and TiO_2 according to their point of zero charge) exhibit only low-temperature desorption peak centered at about 100 °C, whereas TPD profiles of more basic supports (Al_2O_3 and HTC) contain also second desorption peak at higher temperatures (peaks centered at 296 and 208 °C for Al_2O_3 and HTC, respectively). The amount of CO_2 desorbed from the supports increases in the following sequence: TiO_2 < SBA–15 < Al_2O_3 < HTC (see Table 3). The order follows the basicity of the supports; the larger CO_2 amount in the case of SBA-15 can be caused by its much larger surface area in comparison with TiO_2. The TPD profiles varied greatly when vanadium was supported on the individual oxide carriers. The presence

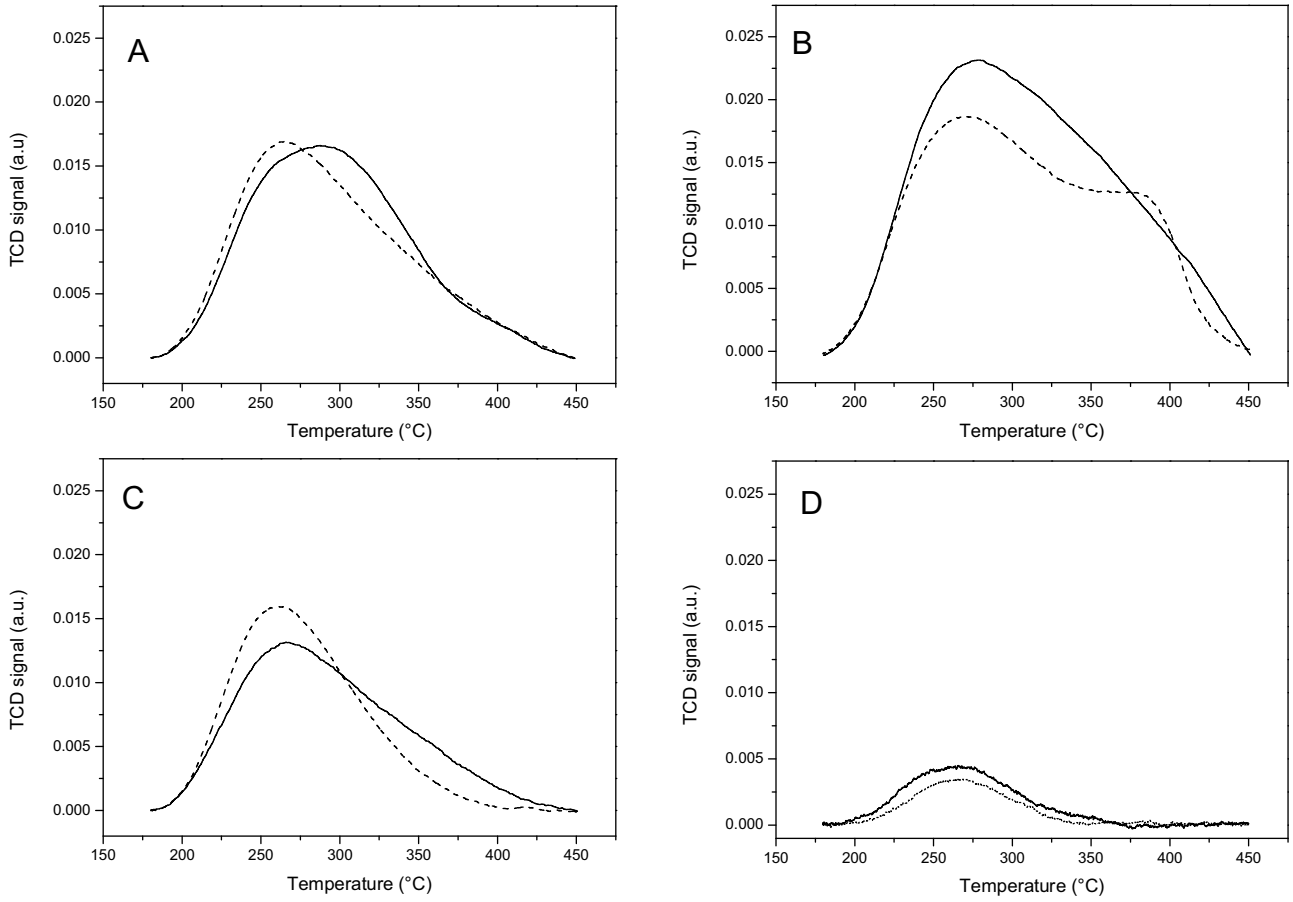

Fig. 6. NH_3-TPD profiles of catalysts (dashed lines) and corresponding support (full lines). (A) V/Al_2O_3, (B) V/TiO_2, (C) V/HTC and (D) V/SBA-15.

of vanadium on the acidic supports increases distinctly the amount of desorbed CO_2 molecules. In the case of V/SBA-15, weak basic sites are generated as indicated by a TPD peak centered at 131 °C. In the case of V/TiO_2, there is only one very broad desorption peak observed indicating the presence of basic sites of medium strength (TPD peak centered at 262 °C). Contrarily, the presence of vanadium on basic supports (Al_2O_3 and HTC) led to a slight decrease in the amount of CO_2 desorbed and the maxima of the desorption peaks shifted to lower desorption temperatures.

3.2. Catalytic tests

Two groups of tests were carried out and the resulting conversions and selectivities are reported in Figs. 8 and 9 and Table 4. In Figs. 8 and 9 the catalysts are organized in the following order: metal oxides without vanadium followed by metal oxides with vanadium and then mesoporous SBA-15 and V/SBA-15. The last one was the blank reaction without catalyst.

The first group of experiments included the use of the supports Al_2O_3, TiO_2, SBA-15 (mesoporous SiO_2) and hydrotalcite. The aim was to obtain information about the individual activity of each support without vanadium depending on the temperature of the reaction. At 150 °C, the most active support was the TiO_2 providing ethanol conversion of about 6%wt. At 250 °C, the most active catalysts were the Al_2O_3 and TiO_2 affording ethanol conversion of ca. 18 and 17%wt., respectively (Fig. 8). The selectivities to acetaldehyde (AA) were higher than 75% when the conversions were higher than 17%wt. Partial oxidation of ethanol to acetaldehyde was found to be the main reaction for all supports. In general, it can be concluded for the supports that the production of AA is favoured when the total conversion of ethanol is higher. The results obtained using titanium oxide could be compared with those obtained by Idriss et al. [44]. They tested TiO_2, CaO, Fe_2O_3 and SiO_2 for the partial oxidation of

Table 3
Temperature programmed reduction and desorptions characteristics.

Material	H_2-TPR		NH_3-TPD		CO_2-TPD	
	T_{max} (°C)	e^-/V	T_{max} (°C)	n_{NH3} (μmol/g)	T_{max} (°C)	n_{CO2} (μmol/g)
V/Al_2O_3	540	1.6	263	110	95, 256	93
Al_2O_3	–	–	288	117	100, 296	150
V/TiO_2	516, 718	2.1	269, 386	162	98	169
TiO_2	–	–	276	186	262	24
V/HTC	685	1.3	261	87	102, 208	358
HTC	–	–	266	90	165	319
V/SBA-15	637	2.0	263	8	131	149
SBA-15	–	–	265	12	155	94

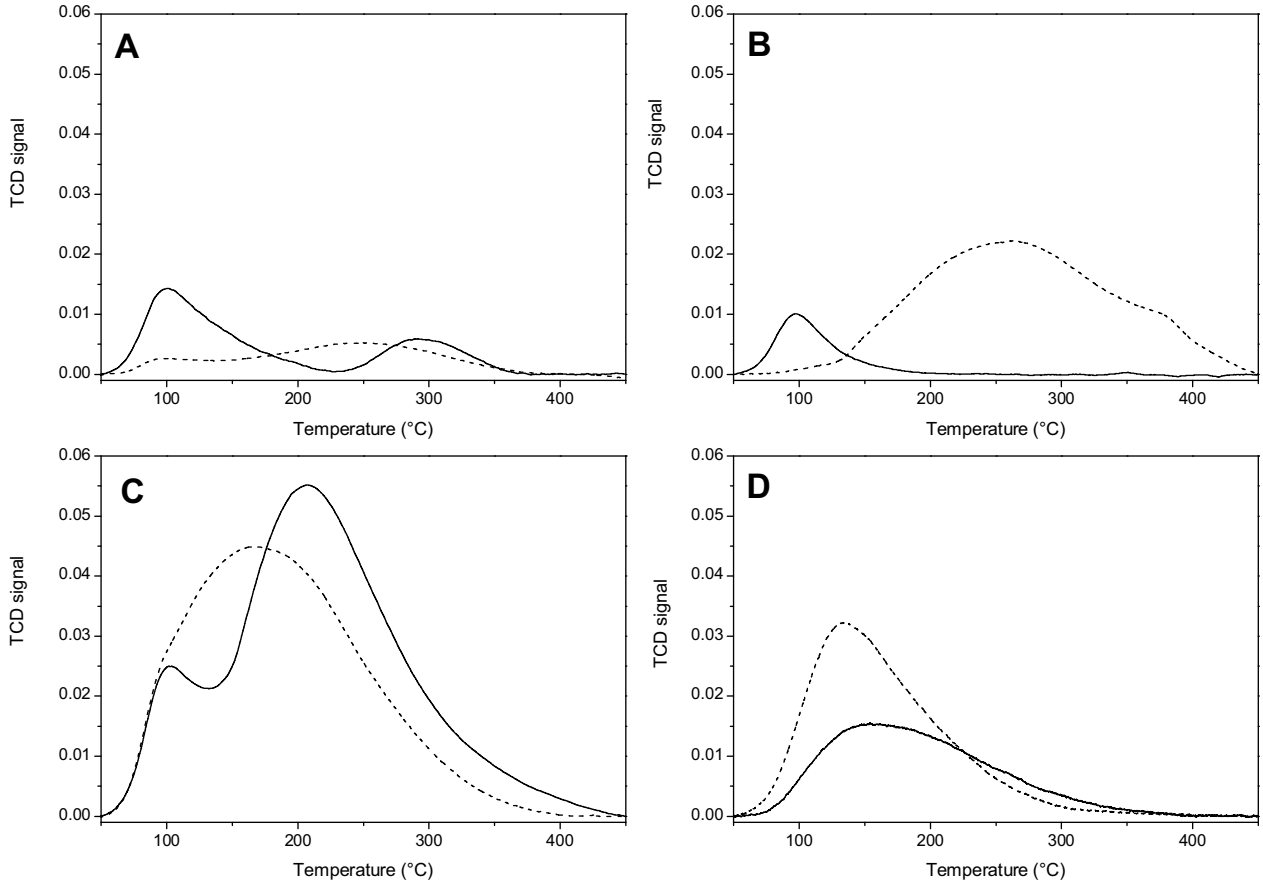

Fig. 7. CO_2-TPD profiles of catalysts (dashed lines) and corresponding support (full lines). (A) V/Al_2O_3, (B) V/TiO_2, (C) V/HTC and (D) V/SBA-15.

ethanol obtaining the highest yields for the Fe_2O_3 and the lowest ones for the SiO_2 (the conversion was negligible at 200 or 250 °C). In comparison, in our experiment the yields obtained using the TiO_2 were much higher which can be explained by the use of different experimental conditions.

To the best of our knowledge, hydrotalcite (HTC) was used, for the first time, as catalyst in the partial oxidation of ethanol affording a selectivity of 100%wt. to acetaldehyde at conversions lower than 7%wt. The low activity could be due to the non-acid nature of the hydrotalcite. Due to this low activity and to the molar ratio oxygen/feedstock, the oxidation to acetaldehyde was favoured. Nevertheless, the Al_2O_3 presented low activity and lower selectivity to acetaldehyde than the HTC indicating that the natural acidity of the alumina (similar effect of the support TiO_2) favoured the oxidation to other products. SBA-15, as confirmed by the NH_3-TPD results, presents low acidity. Hence, SBA-15 tests resulted in a selectivity of 100%wt. to acetaldehyde at 150 and 200 °C, but at 225 and 250 °C the selectivity was lower than 100%wt. It can be inferred that the acido-basic character of the supports affected the activity and yield of the desired acetaldehyde.

The second group of experiments was focused on vanadium containing catalysts. Among the vanadium catalysts (Fig. 9), the two most active catalysts were V/Al_2O_3 and V/TiO_2. For V/TiO_2, the activity was studied only at 150 °C as at T > 150 °C a highly exothermic reaction destabilized the experimental conditions and the temperature in the reactor increased from 160 to more than

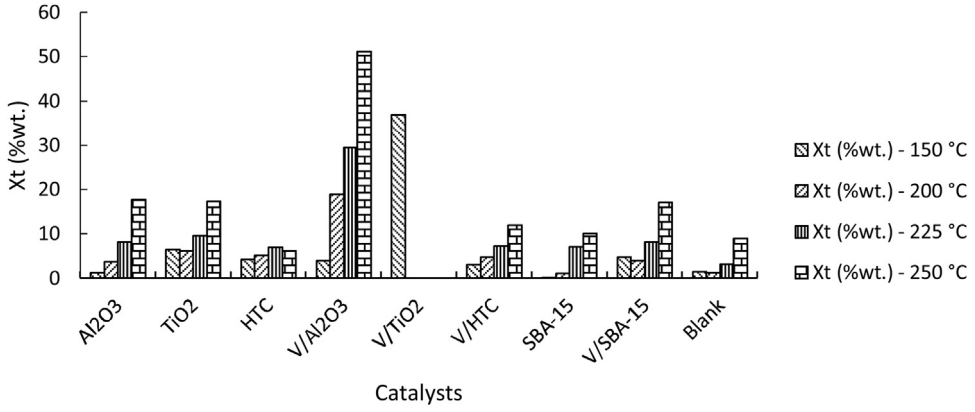

Fig. 8. Total conversions for the partial oxidation of ethanol. Xt (%wt.) is the total conversion by weight.

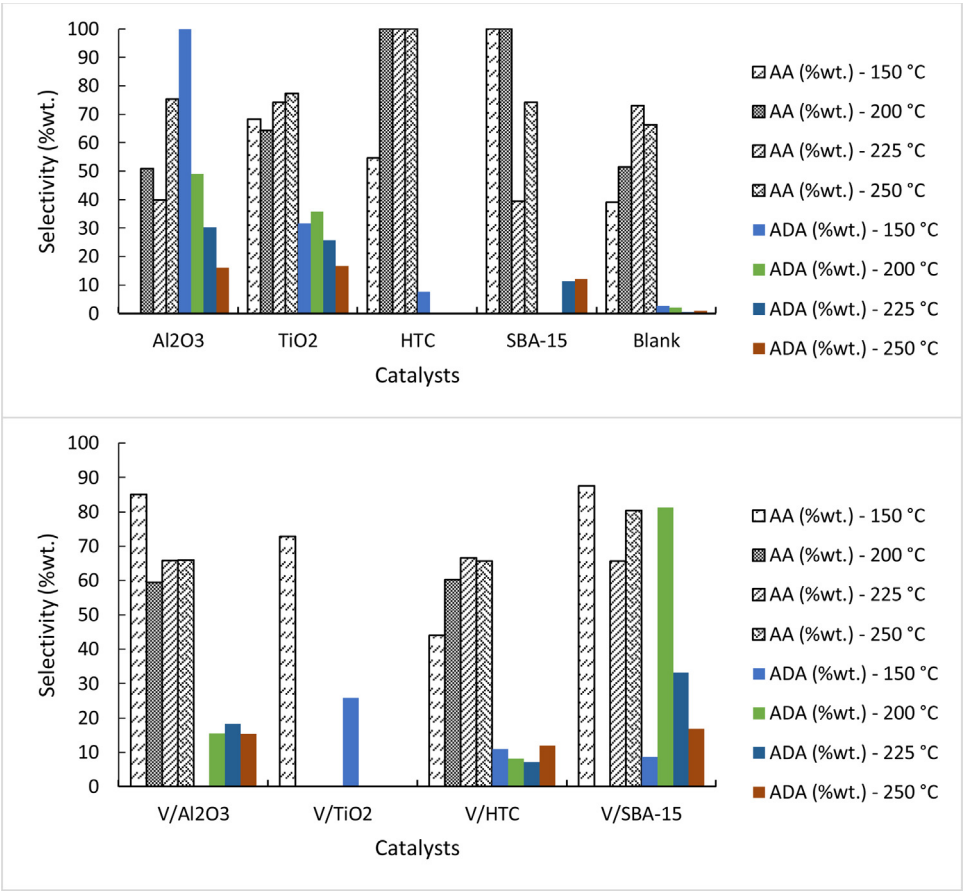

Fig. 9. Selectivities to AA (Acetaldehyde) and ADA (Acetaldehyde Diethyl Acetal) by weight.

400 °C. For V/HTC, the conversion was lower than 12%wt. in all cases. Nevertheless, the highest yields to AA were found for this catalyst at 200–250 °C. The highest yield to acetaldehyde diethyl acetal (ADA) was found for the mesoporous V/SBA-15 catalyst. Interestingly, the most porous material presented the highest yields to the higher molecular weight product. Nevertheless, this activity to ADA was influenced by the addition of vanadium to the SBA-15 support.

Theoretically, the ideal amount of molecular oxygen (according to the stoichiometry) for obtaining a mole of AA from a mole of ethanol is a half mole. In our experimental conditions, the amount of moles of molecular oxygen was approximately a half of the amount of ethanol. So, the total oxidation of ethanol was limited by the amount of oxygen. Nonetheless, to investigate the effect of O_2/ethanol ratio, V/Al_2O_3 and V/TiO_2 were also tested with 5 and 10 NL/h of air flow rate while keeping ethanol feed rate constant. For the test with V/TiO_2, when the amount of oxygen increased two times the selectivity to AA decreased more than 50% indicating that (in this case) the first oxidation to AA was the easiest step of oxidation of ethanol. For V/Al_2O_3 catalyst was also found a decrease of the selectivity to AA. So, the selectivity to oxidation of ethanol to acetaldehyde was larger than the selectivity to the consecutive oxidation of acetaldehyde to acetic acid or other products (Fig. 10).

All results from all the tests carried out are summarized in Table 4. Also in blank tests oxidation of ethanol was observed. Nevertheless, the total conversion was lower than 2% at 150 and 200 °C and 3.1% at 225 °C. At 250 °C the total conversion was 9% which was higher than the activity found for catalysts SBA-15 or HTC increasing the difficulty of studying their activity. A possible origin of this activity could be the presence of iron oxide in the stainless steel which could act as a catalyst [42–44]. The lower activity found for HTC or SBA-15 tests could be due to their influence in the inhibition of the production of acetic acid. Nevertheless, these hypotheses could not be yet proven. The production of 1,3,5 Trioxane (detected by GC–MS) was not described previously in literature as a product of the partial oxidation of ethanol. Nevertheless, in the products, its amount was much lower compared to the amount of acetaldehyde or aldehyde diethyl acetal.

The production of ADA could be favoured by the understoichiometric concentration of molecular oxygen. This low amount inhibited oxidation of AA to other products but the production of ADA only needed the presence of acid sites, ethanol and AA [30]. So, the conditions favoured the production of AA and ADA instead of other products. The most acidic metal oxide catalysts Al_2O_3 and V/Al_2O_3 yielded the largest amount of ADA. In the case of the test using V/SBA-15 a high amount of ADA was obtained. These results could be explained by the mechanism proposed by B. Beck et al. [9] in which the vanadium active sites produced additional Bronsted acidity during the reaction (reduction of vanadium oxide generating "—OH" from "O" bonded to vanadium atoms).

The high activity of the V/TiO_2 catalyst at low temperature was a motivation for performing a long term test for a better understanding of its stability. In fact, the activity of this catalyst at low temperature exceeded the catalytic activity in ethanol dehydrogenation reported in other works [45–47]. Also, the space velocity used in this case was much higher than the one used normally in other tests described in literature [48,49].

Catalyst V/TiO_2 was tested during 212 h (Fig. 11) at 150 °C. Conversion and selectivities were stable affording a total conversion of 61%wt. at TOS = 152 h. The conversion was approximately 60% and the selectivity between 76 and 78% at 56–188 h. The differences in the conversion vs. the time could be due to the adsorption of ethanol

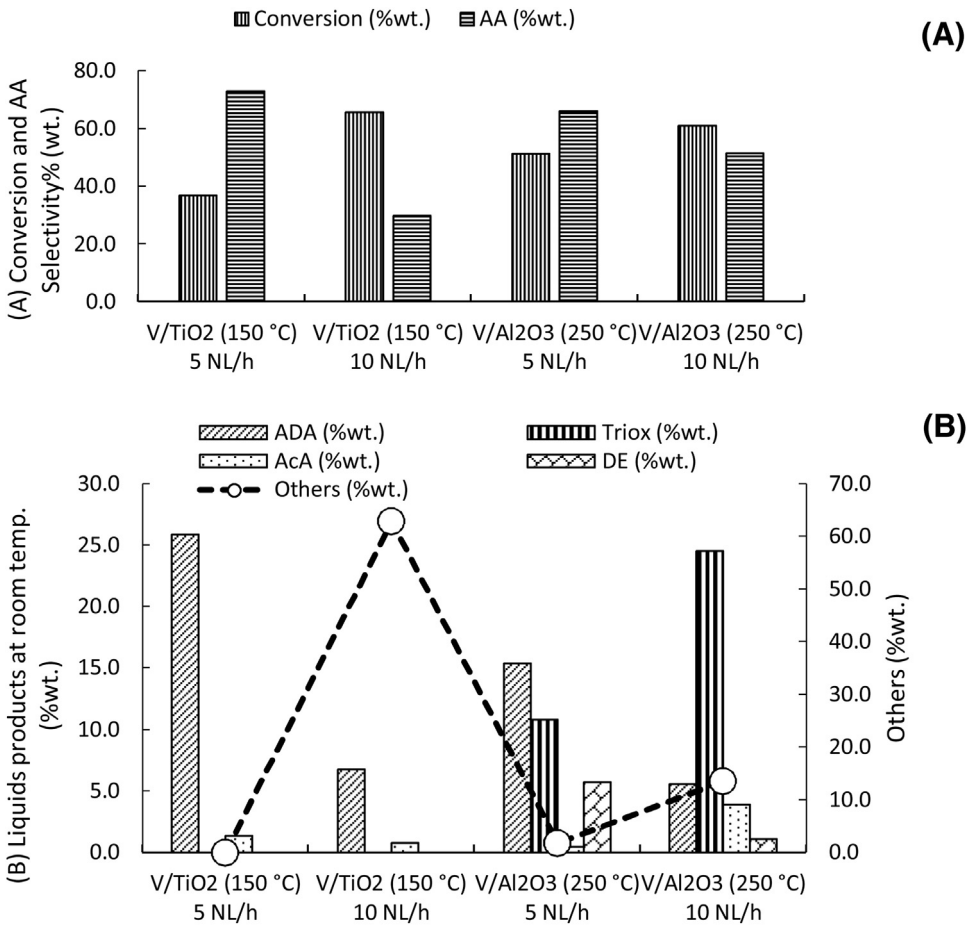

Fig. 10. (A) Ethanol conversion and selectivity to acetaldehyde (AA) at 5 and 10 NL/h gas flow rates at 150 and 250 °C. (B) Selectivities over the V/TiO_2 and V/Al2O3 catalysts at 150 and 250 °C respectively. ADA (Acetaldehyde Diethyl Acetal); Triox (1,3,5 Trioxane); AcA (Acetic Acid); DE (Diethyl Ether); Others. Each measurement was carried out at TOS = 3 h.

and AA over the surface which reacted to form ADA because when the conversion decreased the selectivity to ADA increased.

The comparison of the activity of supports and supports impregnated with vanadium provides clear evidence of the catalytic role of vanadium in these catalysts. Moreover, it can be inferred that surface vanadyl species are the active sites since the V/HTC where vanadium is mainly in the form of magnesium vanadates affords only low conversion of ethanol comparable with the neat support. The characterization by spectroscopic methods indicates the presence of V_2O_5 microcrystallites in V/Al_2O_3 and V/TiO_2, but their concentrations are low and no conclusions about their catalytic activity can be drawn. On the other hand, it is obvious that there are monomeric and oligomeric tetrahedral species present in V/TiO_2, V/SBA-15, V/Al_2O_3. While the spectral data suggest that there are some differences in the population of these centers, the interference from the supports makes their quantification (with

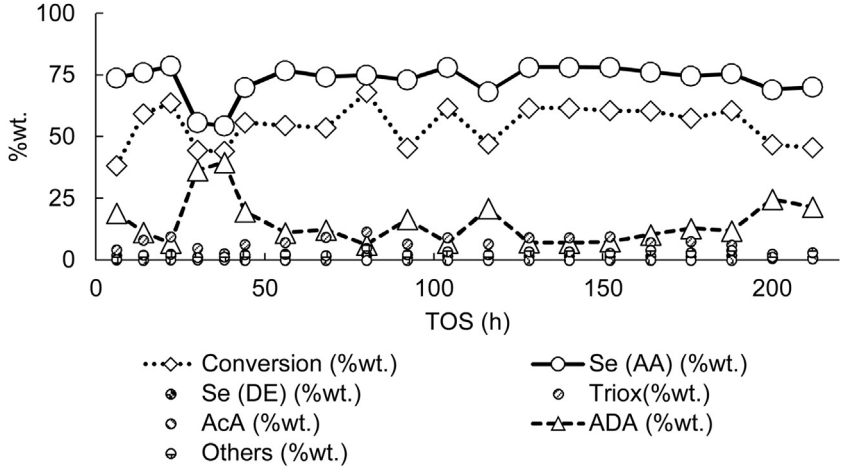

Fig. 11. Long term test for the catalyst V/TiO_2. T = 150 °C; 5 NL/h air flow rate; 1 g of catalyst; 5 g/h Ethanol flow rate.

Table 4
Total conversions and selectivities (%wt.) obtained for all tests (also for blank reaction). AA (Acetaldehyde); ADA (Acetaldehyde Diethyl Acetal); Triox (1,3,5-Trioxane); AcA (Acetic Acid); DE (Diethyl Ether); Others. All measurements were carried out at TOS = 3 h.

Catalyst	Al2O3	TiO_2	HTC	V/Al2O3	V/TiO_2	V/HTC	SBA-15	V/SBA-15	Blank
T = 250 °C									
Total Conversion (%wt.)	17.71	17.30	6.21	51.21	–	11.94	10.13	17.00	8.96
AA (%wt.)	75.32	77.45	100.00	65.98	–	65.62	74.13	80.42	66.38
DE (%wt.)	5.76	5.92	0.00	5.67	–	0.00	0.00	0.00	0.06
Triox (%wt.)	0.00	0.00	0.00	10.77	–	0.27	2.02	2.64	2.72
AcA (%wt.)	2.75	0.00	0.00	0.43	–	1.43	11.69	0.12	29.69
ADA (%wt.)	16.17	16.63	0.00	15.34	–	11.99	12.16	16.82	0.82
Others (%wt.)	0.00	0.00	0.00	1.82	–	20.69	0.00	0.00	0.33
T = 225 °C									
Total Conversion (%wt.)	8.12	9.63	6.96	29.46	–	7.19	7.07	8.09	3.08
AA (%wt.)	39.78	74.27	100.00	65.76	–	66.54	39.45	65.71	73.06
DE (%wt.)	29.99	0.00	0.00	7.87	–	0.00	0.00	0.00	0.26
Triox (%wt.)	0.00	0.00	0.00	6.14	–	4.97	49.28	1.18	2.23
AcA (%wt.)	0.00	0.00	0.00	0.40	–	0.20	0.00	0.00	23.69
ADA (%wt.)	30.23	25.73	0.00	18.31	–	7.16	11.27	33.11	0.43
Others (%wt.)	0.00	0.00	0.00	1.51	–	21.13	0.00	0.00	0.33
T = 200 °C									
Total Conversion (%wt.)	3.68	6.14	5.16	18.82	–	4.74	1.01	3.97	1.14
AA (%wt.)	50.98	64.24	100.00	59.42	–	60.25	100.00	0.00	51.60
DE (%wt.)	0.00	0.00	0.00	7.94	–	0.00	0.00	0.00	0.82
Triox (%wt.)	0.00	0.00	0.00	15.48	–	1.96	0.00	18.68	4.85
AcA (%wt.)	0.00	0.00	0.00	0.12	–	0.21	0.00	0.00	39.75
ADA (%wt.)	49.02	35.76	0.00	15.48	–	8.16	0.00	81.32	2.11
Others (%wt.)	0.00	0.00	0.00	1.57	–	29.41	0.00	0.00	0.88
T = 150 °C									
Total Conversion (%wt.)	1.14	6.37	4.14	3.89	36.80	3.07	0.14	4.74	1.45
AA (%wt.)	0.00	68.25	54.73	85.07	72.81	44.11	100.00	87.52	39.02
DE (%wt.)	0.00	0.00	0.00	0.00	0.00	0.00	0.00	0.00	2.49
Triox (%wt.)	0.00	0.00	22.94	6.19	0.00	1.32	0.00	3.85	7.07
AcA (%wt.)	0.00	0.00	14.71	1.16	1.33	0.06	0.00	0.00	45.90
ADA (%wt.)	100.00	31.75	7.63	0.03	25.86	10.87	0.00	8.63	2.75
Others (%wt.)	0.00	0.00	0.00	7.54	0.00	43.64	0.00	0.00	2.77

the exception of V/SBA-15) virtually impossible. Nonetheless, it can be clearly seen that the support affects greatly the performance/activity of these species. As a result, the activity of the vanadyl species on SBA-15 is significantly lower than when these species are supported on TiO_2 and Al_2O_3. It is thus inferred that the binding energy of the vanadyl species to the support is essential since it facilitates the activation of oxygen in the V-O-T (where T stands for Si, Al or Ti) bond that takes part in the oxidation reaction. It is also clear that further investigations with catalysts having controlled distribution of vanadyl species is essential to understand the activity and selectivity of these catalysts in partial oxidation of ethanol.

4. Conclusions

Eight catalysts were characterized and tested in the partial oxidation of ethanol. The vanadyl species observed by spectroscopic methods (Raman and UV-vis) were unambiguously identified as the active species in the partial oxidation of ethanol. The conversion of ethanol was found to depend on the reducibility of these species determined by TPR. The differences in reducibility are clearly caused by the support and its properties. Among the investigated catalysts, V/TiO_2 was the most active catalyst at low temperature (150 °C) outperforming the catalysts reported in the literature up to now. Moreover, it provided a stable activity over a period of nearly 200 h on stream.

In addition, for first time, formation of 1,3,5 Trioxane was observed in this type of reaction. Mg/Al hydrotalcite (with and without vanadium) was also tested for the first time giving us some more information about the partial oxidation of ethanol over basic mixed oxide catalysts. In particular, the exclusive formation of acetaldehyde from ethanol over HTC, though at low conversion of ethanol, is of interest.

Acknowledgements

The publication is a result of the project reg. no. P106/15-19780S which was financially supported by the Czech Science Foundation GA CR. The project has been integrated into the National Programme for Sustainability I of the Ministry of Education, Youth and Sports of the Czech Republic through the project Development of the UniCRE Centre, project code LO1606.

References

[1] S. Baier, M. Clements, C. Griffiths, J. Ihrig, Biofuels Impact on Crop and Food Prices: Using an Interactive Spreadsheet, Board of Governors of the Federal Reserve System, International Finance Discussion Papers Number 967, 2009 http://www.federalreserve.gov/pubs/ifdp/2009/967/ifdp967.htm.
[2] L. Wei, L.O. Pordesimo, C. Igathinathane, W.D. Batchelor, Biomass Bioenergy 33 (2009) 255–266.
[3] J. Rass-Hansen, H. Falsig, B. Jorgensen, C.H. Christensen, J. Chem. Technol. Biot. 82 (2007) 329–333.
[4] Ullmann's Encyclopedia of Industrial Chemistry, Wiley-VCH Verlag GmbH & Co., KGaA Weinheim, 2006.
[5] Chemical Economics Handbook Acetaldehyde, 2013, http://www.ihs.com/products/chemical/planning/ceh/acetaldehyde.aspx.
[6] W.N.M. Piet, V. Leeuwen, Homogeneous Catalysis: Understanding the Art, Kluwer Academic Publishers Dordrecht, 2004.
[7] R.W. McCabe, P.J. Mitchell, Ind. Eng. Chem. Prod. Res. Dev. 22 (1983) 212–217.
[8] Y. Lin, C. Chang, C. Chen, J. Jehng, S. Shyu, Catal. Comm. 9 (2008) 675–679.
[9] B. Beck, M. Harth, N.G. Hamilton, C. Carrero, J.J. Uhlrich, A. Trunschke, S. Shaikhutdinov, H. Schubert, H. Freund, R. Schlogl, J. Sauer, R. Schomacker, J. Catal. 296 (2012) 120–131.
[10] E.A. Redina, A.A. Greish, I.V. Mishin, G.I. Kapustin, O.P. Tkachenko, O.A. Kirichenko, L.M. Kustov, Catal. Today 241 (2015) 246–254.
[11] G. Du, S. Lim, M. Pinault, C. Wang, F. Fang, L. Pfefferle, G.L. Haller, J. Catal. 253 (2008) 74–90.

[12] R.J. Chimentao, J.E. Herrera, J.H. Kwak, F. Medina, Y. Wang, C.H.F. Peden, Appl. Catal. A-Gen. 332 (2007) 263–272.
[13] H. Lina, S. Kaoa, K. Lin, J. Chang, S. Shyua, J. Catal. 224 (2004) 156–163.
[14] S. Kannan, T. Sen, S. Sivasanker, J. Catal. 170 (1997) 304–310.
[15] M. Tóth, E. Varga, A. Oszkó, K. Baán, J. Kiss, A. Erdőhelyi, J. Mol. Catal. A: Chem. 411 (2016) 377–387.
[16] G. Lee, B.S. Kwak, S. Park, M. Kang, J. Mol. Catal. A: Chem. 411 (2016) 377–387.
[17] G. Du, S. Lim, M. Pinault, C. Wang, F. Fang, L. Pfefferle, G.L. Haller, J. Catal. 253 (2008) 74–90.
[18] C. Santra, S. Shah, A. Mondal, J.K. Pandey, A.B. Panda, S. Maity, B. Chowdhury, Microporous Mesoporous Mat. 223 (2016) 121–128.
[19] J.A. Cecilia, C. García-Sancho, J.M. Mérida-Robles, J. Santamaría-González, R. Moreno-Tost, P. Maireles-Torres, Catal. Today 254 (2015) 43–52.
[20] P.R. Makgwane, S.S. Ray, Appl. Catal. A: Gen. 492 (2015) 10–22.
[21] H.Y. Xu, Y.H. Huang, J.P. Li, F. Ma, K.W. Xu, J. Vac. Sci. Technol. A: Vac. Surf. Films 33 (2015), art. no. 061508.
[22] K. Narsimha, B.M. Reddy, P.K. Rao, V.M. Mastikhin, J. Phys. Chem. 94 (1990) 7336–7337.
[23] M. Setnička, P. Čičmanec, E. Tvarůžková, R. Bulánek, Top. Catal. 56 (2013) 662–671.
[24] R. Bulánek, P. Čičmanec, M. Setnička, Physics Procedia 44 (2013) 195–205.
[25] I.E. Wachs, Dalton Trans. 42 (2013) 11762–11769.
[26] B. Fisher, J. Genossar, G.M. Reisner, Solid State Commun. 226 (2016) 29–32.
[27] B. Jørgensen, S.E. Christiansen, M.L.D. Thomsen, C.H. Christensen, J. Catal. 251 (2007) 332–337.
[28] T. Tarek, S.A. Al-Thabaiti, A.O. Alyoubi, M. Mokhtar, J. Alloy Compd. 496 (2010) 553–559.
[29] X. He, H. Liu, Catal. Today 233 (2014) 133–139.
[30] D.G. Morrell, Catalysis of Organic Reactions, Marcel Dekker Inc., USA, 2003, ISBN 0-8247-4132-3.
[31] O. Kikhtyanin, L. Hora, D. Kubička, Catal. Commun. 58 (2015) 89–92.
[32] A. Zukal, J. Pastva, J. Čejka, Microporous Mesoporous Mat. 167 (2013) 44–50.
[33] R. Bulánek, L. Čapek, M. Setnička, P. Čičmanec, J. Phys. Chem. C 115 (2011) 12430.
[34] X. Gao, P. Ruiz, Q. Xin, X. Guo, B.J. Delmon, J. Catal 148 (1994) 56.
[35] C. Tellez, M. Abon, J.A. Dalmon, C. Mirodatos, J. Santamaria, J. Catal 195 (2000) 113.
[36] M. Setnička, R. Bulánek, L. Čapek, P. Čičmanec, J. Mol. Catal. A: Chem. 344 (2011) 1–10.
[37] R. Bulánek, A. Kalužová, M. Setnička, A. Zukal, P. Čičmanec, J. Mayerová, Catal. Today 179 (2012) 149–158.
[38] C. Pak, A.T. Bell, T.D. Tilley, J. Catal 206 (2002) 49.
[39] L. Mahoney, T. Ranjit, T. Koodali, Materials 7 (2014) 2697–2746.
[40] J.M. López Nieto, A. Dejoz, M.I. Vazquez, Appl. Catal. A 132 (1995) 41.
[41] J.A. Valverde, A. Echavarría, J. Eon, A.C. Faro, L.A. Palacio, Kinet. Mech. Cat. 111 (2014) 679.
[42] A. Dejoz, J.M. López Nieto, F. Melo, I. Vázquez, Ind. Eng. Chem. Res. 36 (1997) 2588.
[43] C.A. Carrero, C.J. Keturakis, A. Orrego, R. Schomäcker, I.E. Wachs, Dalton Trans. 42 (2013) 12644–12653.
[44] H. Idriss, E.G. Seebauer, J. Mol. Catal. A: Chem. 152 (2000) 201–212.
[45] E.A. Redina, A.A. Greish, I.V. Mishin, G.I. Kapustin, O.P. Tkachenko, O.A. Kirichenko, L.M. Kustov, Catal. Today 241 (2015) 246–254.
[46] J.L. Lakshmi, N.J. Ihasz, J.M. Miller, J. Mol. Catal. A: Chem. 165 (2001) 199–209.
[47] E. Santacesaria, A. Sorrentino, R. Tesser, M. Di Serio, A. Ruggiero, J. Mol. Catal. A: Chem. 204–205 (2003) 617–627.
[48] H. Lin, S. Kao, K. Lin, J. Chang, S. Shyu, J. Catal. 224 (2004) 156–163.
[49] I. Abdullahi, T.J. Davis, D.M. Yun, J.E. Herrera, Appl. Catal. 469 (*2014*) 8–17 (49).